Molecular Crystals and Liquid Crystals Science and Technology. Section A. Molecular Crystals and Liquid Crystals

Publication details, including instructions for authors and subscription information:
http://www.tandfonline.com/loi/gmcl19

# Theoretical Studies of Magnetic Orderings in the β- and γ-Phases of P-NPNN and Related Nitroxides

M. Okumura [a] , W. Mori [b] & K. Yamaguchi [a b]

[a] Department of Chemistry, Faculty of Science, Hokkaido University, Sapporo, 060, Japan

[b] Department of Chemistry, Faculty of Science, Osaka University, Toyonaka, Osaka, 560, Japan

Version of record first published: 24 Sep 2006.

To cite this article: M. Okumura , W. Mori & K. Yamaguchi (1993): Theoretical Studies of Magnetic Orderings in the β- and γ-Phases of P-NPNN and Related Nitroxides, Molecular Crystals and Liquid Crystals Science and Technology. Section A. Molecular Crystals and Liquid Crystals, 232:1, 35-44

To link to this article: http://dx.doi.org/10.1080/10587259308035696

*Mol. Cryst. Liq. Cryst.* 1993, Vol. 232, pp. 35–44
Reprints available directly from the publisher
Photocopying permitted by license only

Printed in the United States of America



# THEORETICAL STUDIES OF MAGNETIC ORDERINGS IN THE β- AND γ-PHASES OF P-NPNN AND RELATED NITROXIDES

M. OKUMURA,[a)] W. MORI[b)] AND K. YAMAGUCHI[a,b)]
a) Department of Chemistry, Faculty of Science, Hokkaido University, Sapporo 060, Japan,
b) Department of Chemistry, Faculty of Science, Osaka University, Toyonaka, Osaka 560, Japan

Abstract Intermolecular spin alignment rules are derived on the basis of ab initio results obtained for clusters of triplet carbenes, free radicals, etc. Interrelationships between several theoretical models are also clarified. The APUHF calculations are performed for radical pairs in the β- and γ-phase crystals of para-nitrophenyl nitronyl nitroxide. The magnetic transition temperatures are calculated by the use of Langevin-Weiss type mean-field theory combined with the calculated effective exchange integrals. The origins of ferromagnetic interactions in both the phases are discussed in relation to the intermolecular spin alignment rules.

## INTRODUCTION

Theoretical calculations of effective exchange interactions between radical groups provide a useful guide for molecular design of high-spin molecules[1] and crystaline organic ferromagnets.[2] Previously, unrestricted Hartree-Fock (UHF) molecular orbital (MO) calculations[3] have been carried out for elucidation of effective exchange interactions between organic radicals such as triplet carbenes,[4] nitroxides,[5,6] etc. The UHF Møller-Plesset (MP) type (UHF MP = UMP) calculations have been carried out for their clusters in order to elucidate the correlation corrections for the through-space interaction modes. The basis set dependency of the effective exchange integrals for these clusters has been also examined at the n-th order UMPn (n=1-4) and approximately spin projected (AP) UMPn

(APUMPn) levels of the post Hartree-Fock theory.[2-4] Here , we summarize important aspects revealed by these ab initio and semiempirical calculations in relation to spin alignment rules for radical clusters. The organic ferromagnetisms observed by Kinoshita and his research group[7-10] for para-nitrophenyl nitronyl nitroxide (p-NPNN) are explained by the spin alignment rules on the basis of the extended McConnell model.[11,12]

## EXTENDED McCONNELL MODEL AND SPIN ALIGNMENT RULES

### Intramolecular Spin Polarization (SP) and Spin Delocalization (SD) Mechanisms

According to the first McConnell rule[11] toward organic ferromagnets, component radicals should have the negative spin densities induced by the spin polarization (SP) effect. Let us first consider the introduction of a radical group (R) into a closed-shell molecule. For example, the introduction of α-nitronyl nitroxide into the para-position of nitrobenzene provides para-nitrophenyl nitronyl nitroxide (p-NPNN). The ground (G) configuration of such species is expressed by the HOMO, LUMO and SOMO of fragments as illustrated in A of Fig. 1. The SP configuration is described by the triplet excitation from HOMO to LUMO induced by the SOMO-spin of radical group as illustrated in B of Fig. 1. On the other hand, the spin delocalization (SD) effects are expressed by the intramolecular charge-transfer (CT) configurations in C and D of Fig. 1. The electronic structures of radical species are given by the spin-restricted configuration interaction (CI) form with these configurations as

$$\Phi = D_G \Phi_G + D_{SP} \Phi_{SP} + D_{SDI} \Phi_{SDI} + D_{SDII} \Phi_{SDII} \qquad (1)$$

where $D_X$ denotes the CI coefficient of the configuration X.

The positive and negative alternating spin densities are induced by the product term

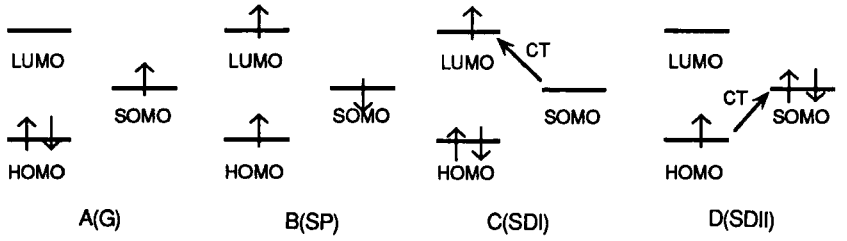


FIGURE 1 The ground(G), spin polarization(SP) and spin delocalization(SD) configurations for radical species

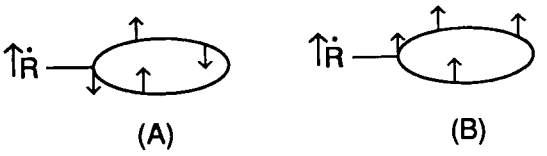


FIGURE 2 Spin density population by the SP(A) and SD(B) effects

($D_G D_{SP}$) between the G and SP configurations as illustrated in A of Fig. 2. On the other hand, the positive spin densities are induced by the product term ($D_G D_{SD}$) between the G and SD configurations as shown in B of Fig. 2. Both the SP and SD configurations can be included by the spin unrestricted Hartree-Fock (UHF) calculation of the whole molecule as has been elucidated by Anderson.[13] In fact, the spin-projected UHF solution is expressed by the spin-restricted CI form like eq. 1.[14] The SP effect is also responsible for the energy splitting between the HOMOs of the up- and down-spins as discussed previously.[5,6]

Intermolecular Spin Alignment Rules

We have carried out the spin-projected UHF calculations of diradicals and polyradicals in the past decades.[1-6] These computations have revealed that there are two different intermolecular approaches: one is a perpendicular approach which exhibits a ferromagnetic interaction and the other is a parallel one with antiferromagnetic interaction. The high-spin or low-spin clusters are formed by the through-space couplings of intrinsic spin in the SOMO (NBMO), induced spin by the spin polarization (SP) mechanism, or induced spin by the spin delocalization mechanism. The magnitudes of the intermolecular effective exchange couplings (Jab) between these spins are classified into three cases as summarized in Table1. Our computational results[4-6] for these three cases are generally explained by the spin alignment rules based on the SP and SD mechanisms[1-6] as summarized in Table 2. Figure 3 illustrates schematically typical types of through-space exchange couplings between spins.

The exchange interactions between the orbitals i and j are generally given by[12-14]

$$J_{ij} = K_{ij} - C(S_{ij})^2 \qquad (2)$$

where $K_{ij}$ and $S_{ij}$ denote, respectively, the Coulombic (potential ) exchange integral and overlap integral, and C is a positive constant. Since the overlap integral disappears in the case of perpendicular approach, the potential exchange (PE) interaction between the spins in the SOMO(A) and SOMO(B) of the composite systems (A+B) plays an important role for

TABLE 1 The through-space exchange couplings (Jab) between spins (X,Y)[a)]

| case | X | Y | \|Jab\| |
|---|---|---|---|
| I | intrinsic spin in SOMO(or NBMO) | intrisic spin in SOMO(or NBMO) | large |
| II | intrinsic spin in SOMO(or NBMO) | induced spin by SP(or SD) | medium |
| III | induced spin by SP(or SD) | induced spin by SP(or SD) | small |

a) notations : SP(spin polarization), SD(spin delocalization).

TABLE 2 Intramolecular spin alignment rules[a)]

| Type | X | A.M. | Y | G.S. |
|---|---|---|---|---|
| I | SOMO(NBMO) | per. | SOMO(NBMO) | HS |
| II | SOMO(NBMO) | par. | SOMO(NBMO) | LS |
| III | SOMO(NBMO) | per. | negative IS by SP | LS |
| IV | SOMO(NBMO) | par. | negative IS by SP | HS |
| V | SOMO(NBMO) | per. | positive IS by SD or SP | HS |
| VI | SOMO(NBMO) | par. | positive IS by SD or SP | LS |
| VII | negative IS by SP | per. | negative IS by SP | HS |
| VIII | negative IS by SP | par. | negative IS by SP | LS |
| IX | negative IS by SP | per. | positive IS by SD or SP | LS |
| X | negative IS by SP | par. | positive IS by SD or SP | HS |
| XI | positive IS by SD or SP | per. | positive IS by SD or SP | HS |
| XII | positive IS by SD or SP | par. | negative IS by SD | LS |

a) notations : A.M.: approach models, per. : perpendicular approach, par.: parallel approach ; IS: induced spin, SP : spin polarization, SD: spin delocalization, HS: high spin, LS: low spin, G.S.: ground spin state.

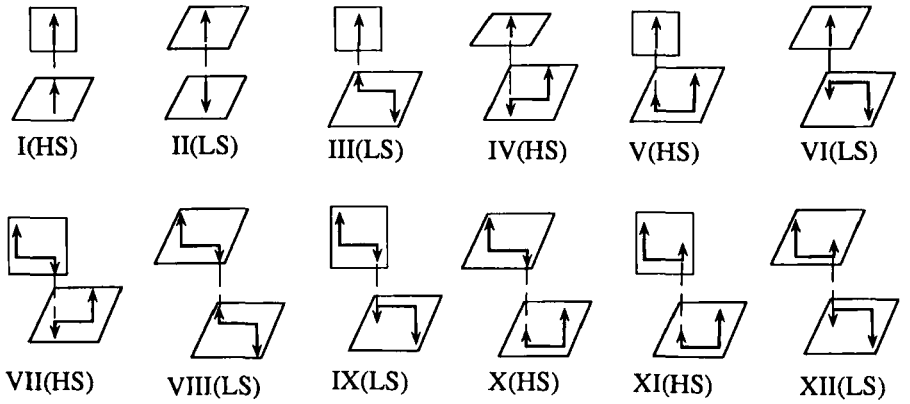


FIGURE 3 Schematic illustration of spin alignment rules based on the APUMP calculations. Small arrows denote the induced spin by SD or SP effects.

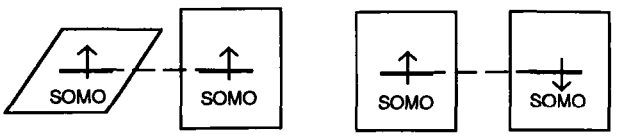


FIGURE 4 potential (PE) and kinetic (KE) exchange interactions between spins in the SOMO(A) and SOMO(B)

the spin alignment as illustrated in Type I of Fig. 4, leading to the high-spin (HS) ground state. On the other hand, the intermolecular SOMO(A)-SOMO(B) overlap term $J_{ij}(OO) = -C(S_{ij})^2$ (namely kinetic exchange (KE) in the Anderson's definition[13]) usually overweighs the PE term in the case of the parallel approach, giving rise to the negative $J_{ij}$. Therefore the ground state becomes the low-spin (LS) in this case as shown in Type II of Fig. 4.

The classification of the perpendicular and parallel approaches is also essential for other cases (Types III-XII) in Fig. 3. For example, Type III expresses the PE interaction between the SOMO(A)-spin and the induced negative spin (B) by the SP effect. Therefore the through-space interaction gives rise to the antiparallel spin alignment of the SOMO-spins as illustrated in Fig. 3, leading to the LS ground state. On the other hand, Type IV expresses the KE interaction between SOMO(A)-spin and induced negative spin (B) by the SP effect. The SOMO-spins align parallel because of this interaction as illustrated in Fig. 3, showing the HS ground state. The so-called McConnell model[11] corresponds to this case. The spin alignment rules are reversed when the SOMO(A)-spin interacts with the induced positive spins by the SD or SP effects as shown in Types V and VI. Types VII-XII show both PE and KE interactions between induced spins by SP or SD. Type X denotes the McConnell-type spin alignment rule. Since the present spin alignment rules involve the McConnell case as examples, they are referred to as the extended McConnell rules.[12,14]

The extended McConnell rules in Fig. 3 can be expressed by the spin-restricted orbital interaction models as illustrated in Figs. 5 and 6. Type III involves the PE interaction between the SOMO(A) and X(B) (X=HOMO or LUMO) since the SP configuration is given by B of Fig. 1, whereas Type IV shows the KE interaction between the SOMO(A) and X(B) (X=HOMO or LUMO). Type IV corresponds to the Awaga-Sugano-Kinishita (ASK) model [15] except for that their next HOMO (NHOMO) is HOMO and NLUMO is LUMO in our notation[12,14]: note that notations of our selection rules are compatible with those of the Woodward-Hoffmann rules for chemical reactions.[16] The orbital interaction schemes in other cases V-XII are obvious as illustrated in Figs. 5 and 6.

## SPIN ALIGNMENTS IN β- AND γ-PHASES OF P-NPNN

Although several formulations are possible to describe the same physical contents[11-15], the spin vector models in Fig. 3 are particularly useful for qualitative explanations of the calculated results by the UHF-based methods. Therefore, later explanations of the APUHF results for p-NPNN are based on this model.

Figure 7 illustrates the spin densities obtained for the planar model compound (**1**) of p-NPNN (**2**) and its related species (**3**) by the INDO UHF method. The alternating up- and down spin densities appear on the nitrobenzene group of **1**, whose bond lengths and angles are assumed and the interplane angles are also assumed to be zero (coplanar). The sum of

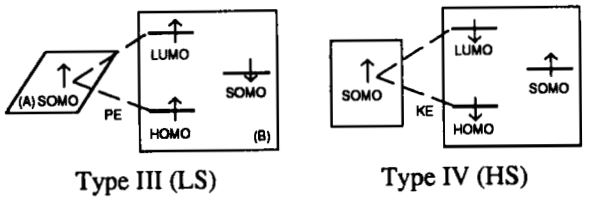


FIGURE 5 Orbital interactions between the SOMO(A) and X(B) (X=HOMO, LUMO) on the basis of the SP( type III, IV) and SD(type V, VI) mechanisms

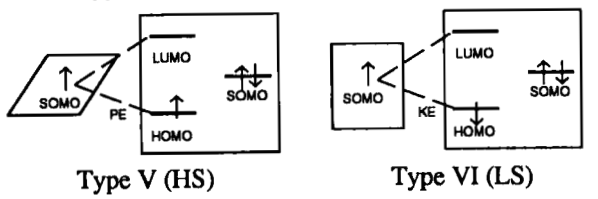


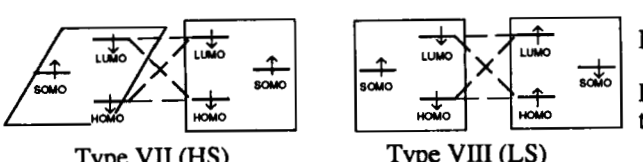


FIGURE 6 Orbital interactions between X(A) and X(B) (X,Y= HOMO, LUMO) on the basis of the SP and SD mechanisms

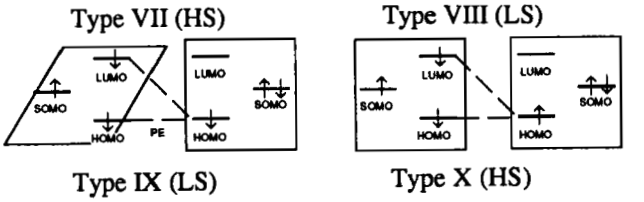


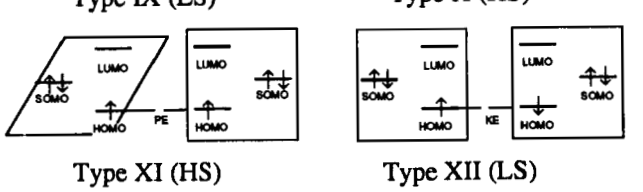


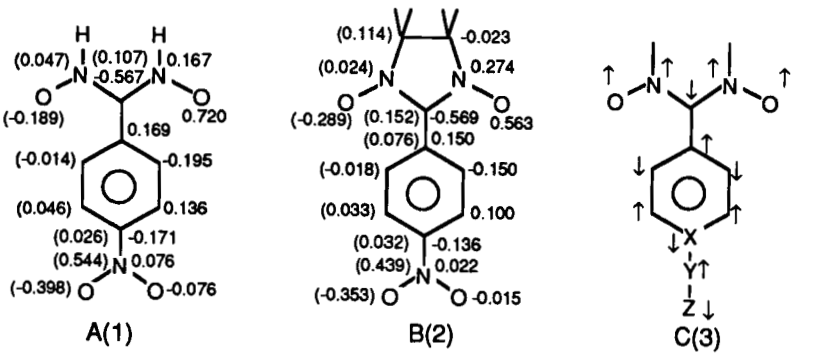


FIGURE 7 Spin density populations (charge densities in parentheses) obtained for p-NPNN and related species by UHF INDO method

all the induced spin densities on the nitro benzene group becomes negative in sign, showing the large SP effect. The tendency of spin density populations is the same for **2**, for which the molecular structure by the X-ray data in the β-phase[7-10] is utilized. Judging from the magnitudes of spin densities calculated for **1** and **2**, they are sensitive to the geometries employed. However, the pattern of the spin density populations is generally expressed by C of Fig. 7 in the case of p-NPNN and related species.

Table 3 summarizes the total energies and effective exchange integrals (J) for pairs of **1** or **2**. The effective exchange integral calculated for the face-to-face dimer of **1** by the APUHF INDO method is -236 $cm^{-1}$ in accord with Type II model. The parallel contact between the central carbon ($C_5$) of the α-nitronyl nitroxide group of the upper **1** and the nitrogen atom ($N_1$) of $NO_2$ group in the lower **1** exhibits the positive J-value (7.16 cm-1), indicating that Type X model works well in this conformation as illustrated in A of Fig. 8. The J-value becomes negative in sign when the $N_1$-atom interacts with the oxygen atom ($O_1$) of a-nitronyl nitroxide group in a parallel manner as illustrated in B of Fig. 8. This corresponds to Type VI. However, the sign of J is reversed with the rotation of $NO_2$ group as shown in C of Fig. 8, since the antiferromagnetic Type VI interaction is suppressed, whereas the ferromagnetic Type V interaction increases. Thus the sign of J is determined by the subtle balance between different type interactions in Fig. 3.

Figure 9A illustrates the Fdd2 crystal structure of β-phase crystal of **2**. There are three independent effective exchange integrals, and total coordination number is twelve.

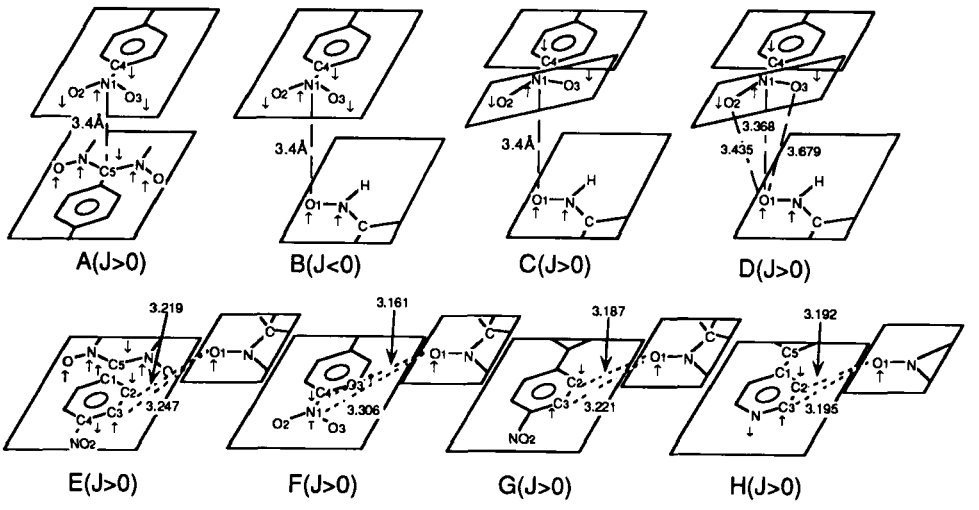


FIGURE 8 Intermolecular interactions between nitroxides : 1(A-C), 2(D-G) and 3 (X=N, Y=Z=none)

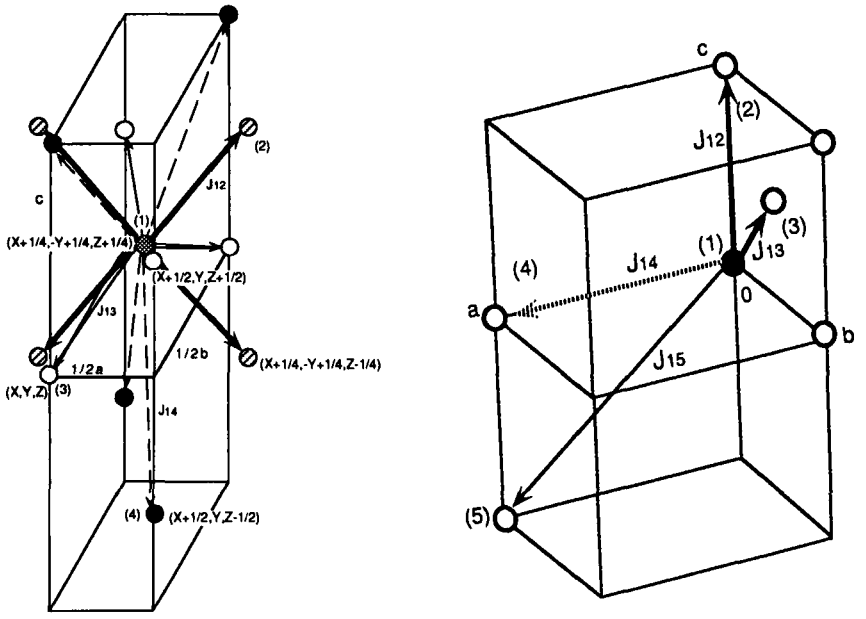


FIGURE 9 Illustrations of crystal structures of β- and γ-phase p-NPNN

TABLE 3 Total energies and total spin angular momentums by UHF INDO and effective exchange integrals by the APUHF methods.

| Compounds | Type[a)] | $^{LS}Et(<S^2>)$ | | $^{HS}Et(<S^2>)$ | | Jab ($cm^{-1}$) |
|---|---|---|---|---|---|---|
| **1** | A | -312.544999 | (3.926) | -312.545033 | (4.927) | 7.46 |
| | B | -312.545954 | (3.921) | -312.545950 | (4.921) | -0.81 |
| | C | -312.824458 | (3.084) | -312.824465 | (4.084) | 1.51 |
| β-phase of **2** | D($J_{12}$) | -409.6935261617 | (2.96941) | -409.693526218 | (3.96941) | 0.167 |
| | E($J_{13}$) | -409.6946502535 | (2.97180) | -409.6946506085 | (3.97180) | 0.078 |
| | ($J_{14}$) | -409.6939716639 | (2.96941) | -409.6939716003 | (3.96941) | -0.014 |
| γ-phase of **2** | F($J_{12}$) | -409.6502337005 | (3.00002) | -409.6502405888 | (4.00014) | 1.511 |
| | G($J_{13}$) | -409.6506581430 | (2.99356) | -409.6506595953 | (3.99357) | 0.319 |
| | ($J_{14}$) | -409.6466116420 | (3.02388) | -409.6466115710 | (4.02388) | -0.016 |
| | ($J_{15}$) | -409.6499334486 | (3.00049) | -409.6499335141 | (4.00049) | 0.014 |

a) see the interaction modes A-G in Fig. 8

Then fours J-values are equivalent as illustrated by the shaded, white and black circles. The three independent J-values were calculated by the APUHF INDO method. They are given in Table 3. The effective exchange integral ($J_{12}$) for the p-NPNN molecules (1) and (2) in Fig.9A is positive since the ferromagnetic Type V interaction is predominant as illustrated in D of Fig. 8. The situation is quite similar to that of C in Fig. 8.

The $J_{13}$-value for the pair of **2** in the positions (1) and (3) in fig. 9A is also positive since the Type IV interaction between the $O_1$-$C_2$ pair overweighs the Type VI interaction for the $O_1$-$C_3$ pair although the $O_1$-$C_2$ distance ($R(O_1$-$C_2)$) is a little longer than the O1-C3 distance $R(O_1$-$C_3)$ as shown in E of Fig. 8: note that the magnitude of the negative spin density on the $C_2$-atom is much larger than that of the positive one on the $C_3$-atom (Fig. 7).

The $J_{14}$-values for the (1,4)-molecular pair is a little negative because the van der Waarls contact between the methyl and nitro groups. However, it does not entail the spin flustration since its magnitude is very small. The ferromagnetic transition tenperature is therefore calculated by the Langevin-Weiss mean field theory[17] in combination with the calculated J-values as

$$k_B T_c = 2/3\ S(S+1)\ (\ 4J_{12} + 4J_{13} + 4J_{14}\ ) \quad (3)$$

Tc is calculated to be 0.66 K, in accord with the observation (0.60 K)[7-10]. The success of the mean field theory in turn indicates that the β-phase of p-NPNN is a three dimensional organic ferromagnet. This is also consistent with the experiment.[7-10]

Figure 9B shows the P1 crystal structure of γ-phase of p-NPNN. The coordination number is eight in this case and four independent J-values are recognized. The $J_{12}$-value for the γ-phase of p-NPNN is positive since the Type IV interaction between the $X(C_4)$ and $O_1$ atomic pair is stronger than the Type VI interaction between the $O_1$-$N_1$-pair as shown in F of Fig. 8 and Table 3.

The $J_{13}$-value for the (1,3)-molecular pair is also positive for the γ-phase since Type IV for the $O_1$-$C_2$ pair overweighs Type VI for the $O_1$-$C_3$ pair (see Fig. 8G). The $J_{13}$-value in the γ-phase is much larger than that of the β-phase because of the relation: $R(O_1$-$C_2) < R(O_1$-$C_3)$. The $J_{13}$-interactions are common for other aromatic nitroxides: for example, see Fig. 8H. The calculated J-values indicate that the γ-phase exhibits the parallel spin alignments within the b-c plane. Unfortunately, the net interplane interaction given by the sum of $J_{14}$ and $J_{15}$ is neagtive (antiferromagnetic), giving rise to the antiferromagnetism at the low tempertature $T_N$ = 0.65 K. The antiferromagnetic transition temperature is calculated by

$$k_B T_N = 2/3\ S(S+1)\ \{\ 2(J_{12} + J_{13}) + 2|(J_{14} + J_{15})|\} \quad (4)$$

$T_N$ is calculated to be 2.61 K, being much higher than the observation. This is quite reasonable since the mean field calculations should overestimate $T_N$ for low-dimensional organic magnets.[17]

## CONCLUSIONS

The spin alignment rules summarized in Table 2 and Fig. 3 are derived on the basis of the UHF and post UHF calculations[1-6] of clusters of triplet carbenes, free radicals, etc. They work well for qualtitative explanations of the sign of the through-space effective exchange integrals calculated for pairs of p-NPNN and related species by the INDO UHF method. The Langevin-Weiss type mean field theory combined with the calculated J-values is also applicable to the theoretical estimation of the ferro- and antiferro-magnetic transition temperatures for the organic crystalline magnets constructed of p-NPNN. The results are quite reasonable as compared with the experiments.[7-10]

However, the present semiempirical study is regarded only as a first step for full understanding of organic ferromagnetisms. The more reliable ab initio calculations of J-values for clusters of p-NPNN are essential for decomposition of intermolecular interaction energies into the contributions of Types I-VI in Fig. 3. The corrections for the mean filed theory are also necessary for quantitative discussions of the transition temperatures.

It is noteworthy that our intermolecular spin alignment rules in Fig. 3, which are derived from the UHF-based post HF calculations, are parallel to the intramolecular spin alignment rules derived fron the same calculations in Fig. 2 of ref. 18.

## ACKNOWLEDGEMENTS

This work was carried out by the aid of the Grant-in-Aid for Scientific Research on Priority Area" Molecular Magnetism" (Area No. 228/04242104) from the Ministry of Education, Science and Culture.

## REFERENCES

1. K. Yamaguchi et al., Synthetic Metals 19, 81, 89 (1987).
2. K. Yamaguchi, N. Namimoto and T. Fueno, Mol. Cryst. Liq. Cryst. 176, 151 (1989).
3. K. Yamaguchi, Chem. Phys. Lett. 33, 330; 35, 230 (1975).
4. K. Yamaguchi, Y. Toyoda and T. Fueno, Chem. Phys. Lett. 159, 459 (1989).
5. K. Yamaguchi et al. Chem. Phys. Lett. 190, 459 (1989).
6. K. Yamaguchi, M. Okumura and M. Nakano, Chem. Phys. Lett. 191, 459 (1989).
7. K. Awaga and Y. Maruyama, J. Chem. Phys. 91, 2743 (1989).
8. M. Kinoshita et al., Chem. Lett. 1225 (1991).
9. P. Turek et al., Chem. Phys. Lett. 180, 327 (1991).
10. Y. Nakazawa et al., Phys. Rev. in press (1992).
11. H. M. McConnell, J. Chem. Phys. 39, 1910 (1963).
12. K. Yamaguchi et al., Chem. Lett. 629 (1986).
13. P. W. Anderson, Solid State Phys. 14, 99 (1963).
14. K. Yamaguchi and T. Fueno, Chem. Phys. Lett. 159, 465 (1989).
15. K. Awaga, T. Sugano and M. Kinoshita, Chem. Phys. Lett. 141, 540 (1987).
16. R. B. Woodward and R. Hoffmann, Angew. Chem. Intern. Ed. 8, 781 (1969).
17. C. Kittel, Introduction to Solid State Phys. p421 (John Wiley & Sons, 1986).
18. M. Okumura et.al., this proceeding in press.